*atmosphere*

MDPI

*Article*

# Tracking the Transport of $SO_2$ and Sulphate Aerosols from the Tonga Volcanic Eruption to South Africa

**Lerato Shikwambana [1,2,*], Venkataraman Sivakumar [3,4] and Kanya Xongo [1]**

1 Earth Observation Directorate, South African National Space Agency, Pretoria 0001, South Africa; kxongo@sansa.org.za
2 School of Geography, Archaeology and Environmental Studies, University of the Witwatersrand, Johannesburg 2050, South Africa
3 School of Chemistry and Physics, University of KwaZulu-Natal, Durban 4041, South Africa; venkataramans@ukzn.ac.za
4 National Institute for Theoretical and Computational Sciences, University of KwaZulu Natal, Durban 4000, South Africa
* Correspondence: lshikwambana@sansa.org.za

**Abstract:** During a volcanic eruption, copious amounts of volcanic gas, aerosol droplets, and ash are released into the stratosphere, potentially impacting radiative feedback. One of the most significant volcanic gases emitted is sulphur dioxide, which can travel long distances and impact regions far from the source. This study aimed to investigate the transport of sulphur dioxide and sulphate aerosols from the Tonga volcanic eruption event, which occurred from the 13th to the 15th of January 2022. Various datasets, including Sentinel-5 Precursor (TROPOMI), the Ozone Monitoring Instrument (OMI), and the Ozone Mapping and Profiler Suite (OMPS), were utilized to observe the transport of these constituents. The TROPOMI data revealed westward-traveling $SO_2$ plumes over Australia and the Indian Ocean towards Africa, eventually reaching the Republic of South Africa (RSA), as confirmed by ground-based monitoring stations of the South African Air Quality Information System (SAAQIS). Moreover, the Cloud-Aerosol Lidar and Infrared Pathfinder Satellite Observations (CALIPSO) demonstrated sulphate aerosols at heights ranging from 18 to 28 km with a plume thickness of 1 to 4 km. The results of this study demonstrate that multiple remote sensing datasets can effectively investigate the dispersion and long-range transport of volcanic constituents.

**Keywords:** volcanic emission; Sentinel-5P; aerosols; $SO_2$; transport



**Citation:** Shikwambana, L.; Sivakumar, V.; Xongo, K. Tracking the Transport of $SO_2$ and Sulphate Aerosols from the Tonga Volcanic Eruption to South Africa. *Atmosphere* **2023**, *14*, 1556. https://doi.org/10.3390/atmos14101556

Academic Editors: Alessia Sannino, Alejandro Rodríguez-Gómez and Simone Lolli

Received: 14 September 2023
Revised: 6 October 2023
Accepted: 11 October 2023
Published: 12 October 2023



## 1. Introduction

Volcanic eruptions are natural phenomena that can have significant impacts on climate, environment, and human health. With approximately 1500 potentially active volcanoes worldwide, understanding the transport of volcanic emissions is crucial for assessing their impact. Volcanic eruptions release a variety of gases and aerosols, including sulfur dioxide ($SO_2$) and volcanic carbon dioxide ($CO_2$), which can affect climate by promoting global warming and cooling, respectively [1]. These emissions can also cause secondary events, such as floods, landslides (if accompanied by precipitation), and wildfires, which further exacerbate their impact. Health impacts of volcanic eruption include suffocation, traumatic injuries, infectious diseases, and respiratory diseases. In particular, volcanic acid rain dominated by hydrochloric and sulfuric acid can harm aquatic environments, agricultural products, and wildlife. To fully comprehend the impact of volcanic emissions, remote sensing datasets and reanalysis data have been utilized to observe the transport and distribution of volcanic materials.

Several studies have assessed the transport and distribution of volcanic emissions. Recently, Vernier et al. [2] studied the distribution of volcanic materials in the lower stratosphere after the Mount Kelud (7.96° S, 112.31° E) eruption that occurred in 2014, where approximately 0.15 Tg of $SO_2$ was measured. Stone et al. [3], Lopes et al. [4], Sangeetha et al. [5], Shikwambana and Sivakumar [6], and Bègue et al. [7] observed the transport of volcanic constituents from the Calbuco (41.2° S, 72.4° W; Chile) volcanic eruption in 2015, where approximately 0.36 Tg of $SO_2$ was measured. Kloss et al. [8] investigated the Raikoke (48.29° N, 153.25° E; Kuril Islands) and Ulawun (5.05° S, 151.33° E; Papua New Guinea) eruptions in 2019, where approximately 0.36 Tg and 1.5 Tg of $SO_2$ were measured for Ulawun and Raikoke, respectively. Recently, Kloss et al. [8] utilized in situ observations (using a light optical aerosol counter (LOAC) on two balloon flights and ground-based (lidar) measurements) of aerosol concentration and size distribution, the optical and micro-physical properties of the aerosols, and satellite data to investigate the stratospheric Hunga Tonga plume. According to Shin et al. [9], volcanic eruptions emit $SO_2$, which is known to increase optical thickness at stratospheric altitudes. Explosive volcanic eruptions directly inject the largest source of sulphate aerosol quantities into the stratosphere. Depending on various factors such as injection height, total mass loading, latitudes, and dispersion pattern, these sulphate aerosols can travel over long distances and persist for extended periods of time [10].

Various satellite sensors have been utilized to examine the distribution and transport of volcanic emissions. Some of the commonly used satellite sensors are Sentinel-5P [11,12], the Ozone Monitoring Instrument (OMI) [13,14], Cloud-Aerosol Lidar and Infrared Pathfinder Satellite Observations (CALIPSO) [15,16], and MODIS [17,18]. However, few studies have used reanalysis data to investigate the distribution of $SO_2$ from volcanic eruptions. Reanalysis data enhance our knowledge of how the factors that impact our climate have changed over time. One advantage of reanalysis is that it can fill gaps in observations in both time and space.

This paper aimed to investigate the transport of $SO_2$ and volcanic aerosols emitted from the Tonga eruption site to South Africa using different remote sensing datasets. To our knowledge, no such studies have been conducted. Specifically, the objectives were to study (1) the length of time the $SO_2$ and the aerosols took to travel to South Africa, (2) the altitudes at which volcanic aerosols were detected over southern Africa, and (3) the impact of the volcanic aerosols and $SO_2$ over southern Africa. By analyzing the distribution of volcanic constituents, we can gain a better understanding of their transport across different altitudes and distances and their potential impact on climate and the environment.

## 2. Description of the Tonga Volcano Eruption

Hunga Tonga–Hunga Ha'apai (Tonga) (20.54° S, 175.38° E) is a submarine volcano in the South Pacific located about 30 km south of the submarine volcano of Fonuafo'ou and 65 km north of Tonga's main island (see Figure 1). Tonga has 21 Holocene volcanoes including volcanoes that have erupted within the past 20 years. More recently, the Tonga volcano erupted on 13 and 14 January 2022 with the largest and explosive eruption occurring on 15 January 2022 at 17:30 local time (4:30 UTC) [19]. It is estimated that the eruption column from the 15 January 2022 eruption may have risen as much as 55–58 km into the Mesosphere [19]. The eruption released tons of ash, dust, and toxic gases into the atmosphere. A detailed description and the impact of the eruption were published in the Global Volcanism Program [19]. In summary, the report showed that ashfall and tsunami had damaged all the islands; dozens of earthquakes, M 4.5–5, were centered in the vicinity of the volcano after the eruption; and, as a result of the ashfall and earthquakes, domestic flights were suspended. It is estimated that ~0.4 megatons of $SO_2$ were released into the stratosphere and this was unlikely to have any global cooling effect. Furthermore, Xu et al. [20] showed that a total amount of 139 $\pm$ 8 Tg of water vapor was injected into the stratosphere and resulted in an increase of 8.9 $\pm$ 0.5% in global stratospheric water vapor.

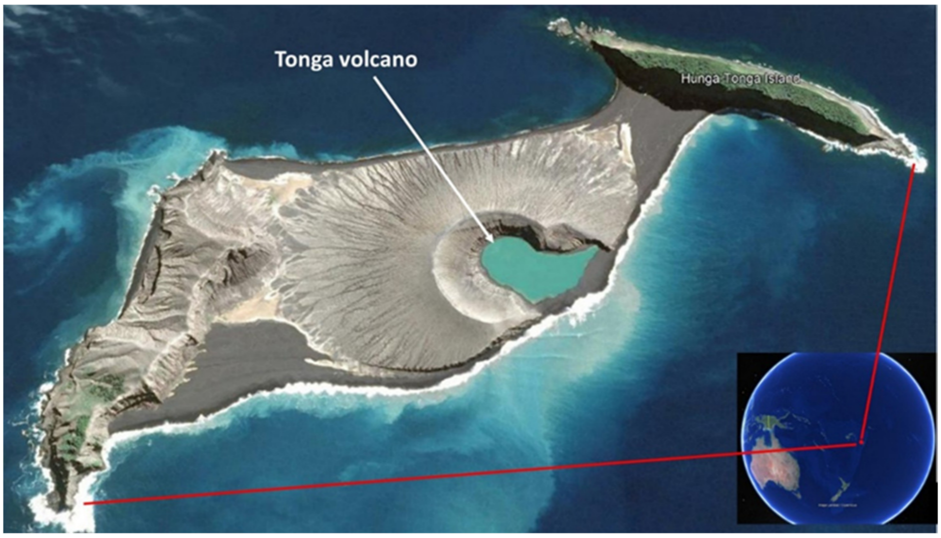


**Figure 1.** Hunga Tonga–Hunga Ha'apai submarine volcano (image retrieved from Google Earth Pro).

## 3. Data

### *3.1. Sentinel-5P/TROPOMI*

Sentinel-5 Precursor (Sentinel-5P) is a Copernicus mission launched in 2017 to monitor the Earth's atmosphere with high spatio-temporal resolution, using the Tropospheric Monitoring Instrument (TROPOMI) near-nadir imaging spectrometer. The mission's objective is to perform atmospheric measurements for air quality, ozone, and UV radiation, and climate monitoring and forecasting. The TROPOMI instrument operates in a push-broom configuration, covering wavelength bands between the ultraviolet and the shortwave infrared, with a swath width of ~2600 km on the Earth's surface. The typical pixel size (near nadir) is $7 \times 3.5$ km$^2$ for all spectral bands, with the exception of the UV1 band ($7 \times 28$ km$^2$) and SWIR bands ($7 \times 7$ km$^2$). The TROPOMI $SO_2$ column density data from 1 January to 5 February 2022 were used in this study. Detailed $SO_2$ retrievals from the TROPOMI are discussed by Theys et al. [11]. Data processing was carried out using Google Earth Engine and Quantum Geographic Information System (QGIS). More information on Sentinel-5P and the TROPOMI can be found in Theys et al. [11], Tilstra et al. [21], and Verhoelst et al. [22].

### *3.2. OMI*

The OMI (Ozone Monitoring Instrument) is an imaging spectrometer launched in 2004 as part of the EOS (Earth Observing System) Aura spacecraft. It measures solar radiation backscattered by the Earth's atmosphere and surface in the wavelength range of 270–500 nm with a spectral resolution of approximately 0.5 nm. The OMI has a nadir viewing configuration and measures 60 cross-track positions or pixels, with varying pixel sizes depending on the track position. The pixel sizes range from $13 \times 24$ km$^2$ at nadir to about $28 \times 150$ km$^2$ at the outermost swath angle.

The OMI provides near-global coverage of solar backscatter radiances in one day (14 orbits), with a revisit time of 1–2 days. It is capable of measuring key air quality components such as nitrogen dioxide ($NO_2$), $SO_2$, and aerosols. It can also map ozone profiles at $36 \times 48$ km and distinguish between different aerosol types, including smoke, dust, and sulphates. In this study, the OMI $SO_2$ column amount data from 1 January to 5 February 2022 were used. The data were obtained through the Giovanni platform, which facilitates access to Earth science data from NASA satellites. More details on the OMI can be found in Boersma et al. [23], Bucsela et al. [24], Levelt et al. [25], and Levelt et al. [26].

### 3.3. OMPS

The Ozone Mapping and Profiler Suite (OMPS) was launched in October 2011. It is aboard the joint NASA/NOAA Suomi National Polar-orbiting Partnership (Suomi NPP) satellite. Near-real-time OMPS products include the total column ozone, vertical ozone profile swath, aerosol index, and $SO_2$. More details on the OMPS are given by Flynn et al. [27] and Yang et al. [28].

### 3.4. CALIPSO

CALIPSO is a satellite mission launched in April 2006, aimed at understanding the impact of aerosols and clouds on the Earth's radiation budget and climate. The mission uses a light detection and ranging (lidar) and imaging system, which includes three co-aligned nadir-viewing payloads: the Imaging Infrared Radiometer (IIR), the Wide-Field Camera (WFC), and the Cloud-Aerosol Lidar with Orthogonal Polarization (CALIOP). CALIOP is a two-wavelength polarization-sensitive lidar that provides high-resolution vertical profiles of aerosols and clouds. The algorithms used to retrieve a variety of optical and microphysical properties from CALIOP data are discussed in detail by Winker et al. [29], while further details on the CALIPSO mission can be found in Winker et al. [30] and Winker et al. [31].

### 3.5. SAAQIS

The South African Air Quality Information System (SAAQIS) is a platform for managing air quality information in South Africa. The SAAQIS aims to ensure that accurate, current, complete, and relevant air quality information is available to stakeholders and the public. The South African Weather Service (SAWS) is the custodian of the SAAQIS. More details on the SAAQIS are given by Gwaze and Mashele [32]. SAAQIS data can be accessed at https://saaqis.environment.gov.za/ (accessed on 26 July 2023). In this study, we have used the $SO_2$ measurements.

## 4. Results

### 4.1. $SO_2$ Observations and $SO_2$ Time Series by TROPOMI

TROPOMI $SO_2$ imagery for the 0–40° S and 10–180° E region, with a spatial resolution of $3.5 \times 5.5$ km, is shown in Figure 2. In the period 6–12 January 2022, a low $SO_2$ column density, less than $1.14 \times 10^{-4}$ mol/m$^2$, was observed by the TROPOMI over the study region. This was prior to the volcanic eruption. However, during the 13–21 January 2022 period, a large plume of $SO_2$ ($4 \times 10^{-4}$ mol/m$^2$) was observed by the TROPOMI travelling from the eruption site and travelling over Australia. During the period of 21–27 January 2022, a large $SO_2$ plume was observed travelling over the Indian Ocean and Madagascar towards southern Africa. Specifically, $SO_2$ reached southern Africa and travelled over the Atlantic Ocean. Most interestingly, sudden $SO_2$ plumes were observed over some parts of the Republic of South Africa (RSA) during the 28 January–5 February 2022 period, which is something generally not seen in those areas.

Figure 3 shows $SO_2$ time series from the volcanic eruption over four sites: Tonga, Australia, the Indian Ocean, and central South Africa. Before 12 January 2022, low $SO_2$ column densities (<0.0005 mol/m$^2$) were observed (see Figure 3a). A strong $SO_2$ peak (0.0037 mol/m$^2$) was suddenly observed on 13 January over the Tonga site due to the eruption. Moderate $SO_2$ peaks (0.00115 mol/m$^2$ and 0.0007 mol/m$^2$) around 22–24 January and 28 January 2022 were also observed. The two peaks imply that two $SO_2$ plumes traveled at different times from the origin site. Low $SO_2$ peaks (<0.00055 mol/m$^2$) were observed between 21–26 January 2022 over the Indian Ocean (see Figure 3c). The low-density column values imply that the $SO_2$ was dissipating as it travelled away from the origin site. On 1 February 2022, a moderate $SO_2$ peak (0.0007 mol/m$^2$) was observed over central South Africa (see Figure 3d), which could have had contributions from surrounding coal power stations, but the major contributor was the volcanic eruption.

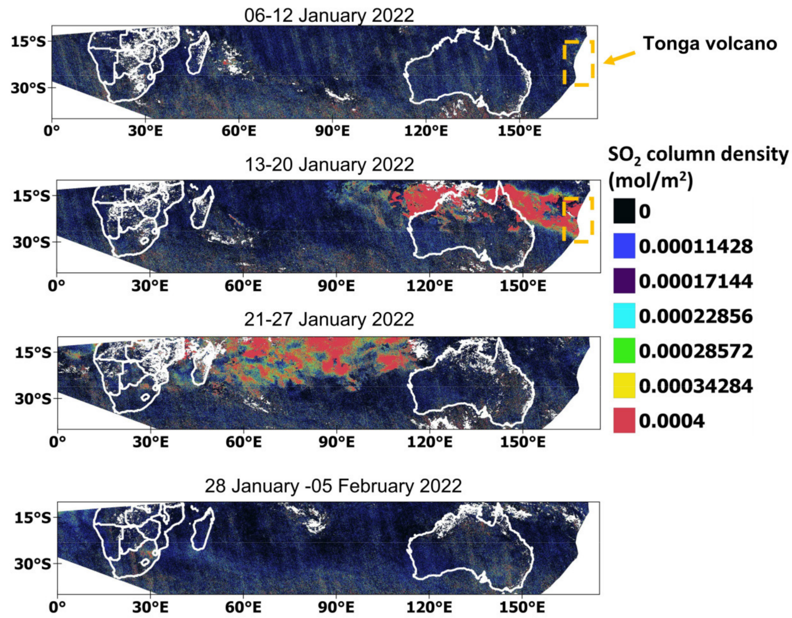


**Figure 2.** Transport of $SO_2$ from the Tonga volcanic eruption observed using TROPOMI.

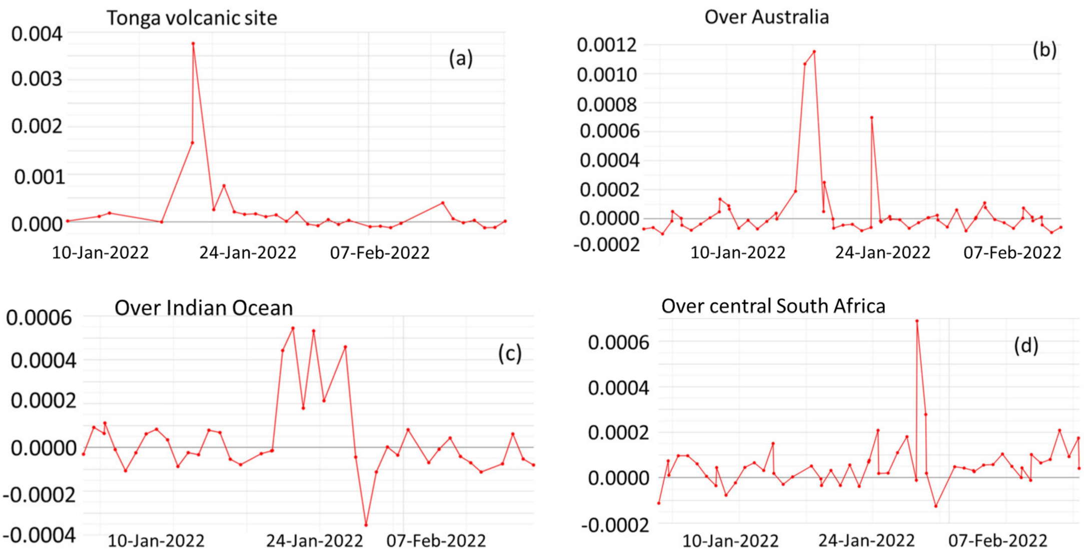


**Figure 3.** Time series of $SO_2$ (mol/m$^2$) retrieved from TROPOMI over (**a**) Tonga volcanic site, (**b**) Australia, (**c**) Indian Ocean, and (**d**) central South Africa.

### *4.2. $SO_2$ Observation and Time Series over RSA Using OMI and Ground-Based Monitors*

The columnar TROPOMI $SO_2$ imagery over the RSA region (20–35° S and 15–35° E) is shown in Figure 4a. The known $SO_2$ hotspots [33,34] are clearly visible in the 01–12 January and 13–26 January 2022 periods. These $SO_2$ hotspots originate from the coal power stations situated in the Highveld of Mpumalanga Province and in Limpopo Province in the RSA. A noticeable dispersion of $SO_2$ (red blocks) in the interior of the RSA and in the eastern part of the RSA is also observed. This unusual $SO_2$ emanated from the Tonga volcanic eruption. Figure 4b shows the OMI $SO_2$ column density time series from 1 January to 10 February 2022 over the RSA region. Generally, low daily $SO_2$ column density (less than 0.04 mol/m$^2$) values were observed from 1–31 January 2022. A temporary increase in $SO_2$ loading (~0.06 mol/m$^2$) was observed on 2 February 2022. This was the $SO_2$ emitted from the volcanic eruption. It is estimated that the $SO_2$ took ~18 days to travel from Tonga to the RSA. Figure 4c shows the $SO_2$ time profiles measured from the ground monitoring stations in the RSA. The $SO_2$ ground monitoring stations in the RSA agreed with the OMI

$SO_2$ observations. $SO_2$ peaks at the Balfour station in Mpumalanga showed the highest $SO_2$ concentration (~90 ppbV) during the overpass of the $SO_2$ on 5 February 2022. Other ground monitoring stations showed a high $SO_2$ concentration, such as the Alexandra station in Gauteng Province at ~40 ppbV on 3 February 2022; Middleburg in Mpumalanga Province and Zamdela in Free State Province both showed $SO_2$ concentrations of ~20 ppbV on 5 February 2022. These results complement each other and give a detailed picture of the transport of $SO_2$ from Tonga.

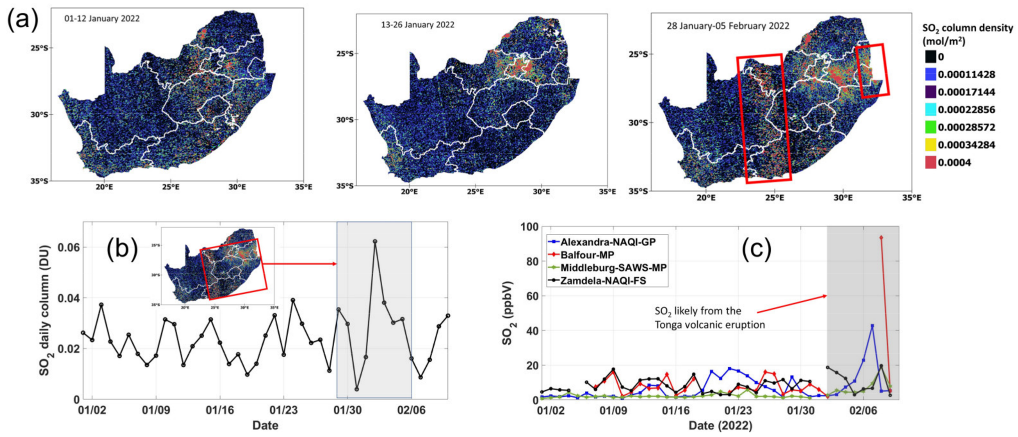


**Figure 4.** (**a**) Spatial distribution of $SO_2$ column density over RSA from 1 January to 5 February 2020. (**b**) OMI $SO_2$ column density time series from 1 January to 5 February 2022 over RSA. (**c**) $SO_2$ concentration from various ground monitoring stations in RSA.

### *4.3. OMPS $SO_2$ Observation and OMI $SO_2$ Time Series*

Figure 5a,b show the lower stratospheric (STL) $SO_2$ column on 18 January and on 23 January 2022, respectively. On 18 January 2022 (see Figure 5a), a high $SO_2$ loading in the lower stratosphere was observed over northern Australia. The $SO_2$ mass was measured at 352.5 kt and the maximum column density was measured at 9.68 DU. In general, air mass is responsible for the transport of gases and aerosols in the atmosphere. In this study, it took the air masses three days to transport the large amount of $SO_2$ from the eruption site to Australia. One of the disadvantages of stratospheric $SO_2$ is its ability to convert into sulfate aerosol which interacts with the long-lived Junge layer [35]. Disappointingly, the dynamics of the Junge layer are still not well understood [35]. Moreover, it is known that stratospheric aerosols are an important climate forcing factor because they modify both the shortwave and longwave radiation in the atmosphere and reaching the Earth's surface [36]. It is speculated that the $SO_2$ plume did not have a major impact over Australia. On 23 January 2022, the OMPS shows that the $SO_2$ plume dissipated to a $SO_2$ mass of 140 kt and a $SO_2$ max column density of 2.79 DU. The dissipation of $SO_2$ in the atmosphere can be caused by several factors such as conversion of $SO_2$ to sulphate and chemical reactions with other atmospheric compounds and/or elements to form new species and chemical reactions with water vapor to form acid rain. Figure 5b further shows $SO_2$ travelling in a westward direction over southern Africa towards the Atlantic Ocean. The observation of moderate $SO_2$ column STL (~1.2 DU) in Africa was observed over Angola and Zambia. A time series of the $SO_2$ daily column over the 0–40° S and 10–180° E region retrieved from the OMI is shown in Figure 5c. A background $SO_2$ column density of ~0.025 DU was present from 1–12 January 2022. The $SO_2$ background is the "normal" $SO_2$ concentration in the absence of an event. However, a sharp increase in $SO_2$ column density (0.31 DU) was observed from 15 to 16 January 2022. This sudden rise in the $SO_2$ loading was due to the large Tonga volcanic eruption that occurred on the 15th of January 2022. The broad peak implies that the $SO_2$ dissipated slowly over time until it reached its background $SO_2$ column density of ~0.025 DU around 28 January 2022. From 28 January to 5 February 2022, a temporary slight increase in $SO_2$ was observed in the RSA (see Figure 3, TROPOMI).

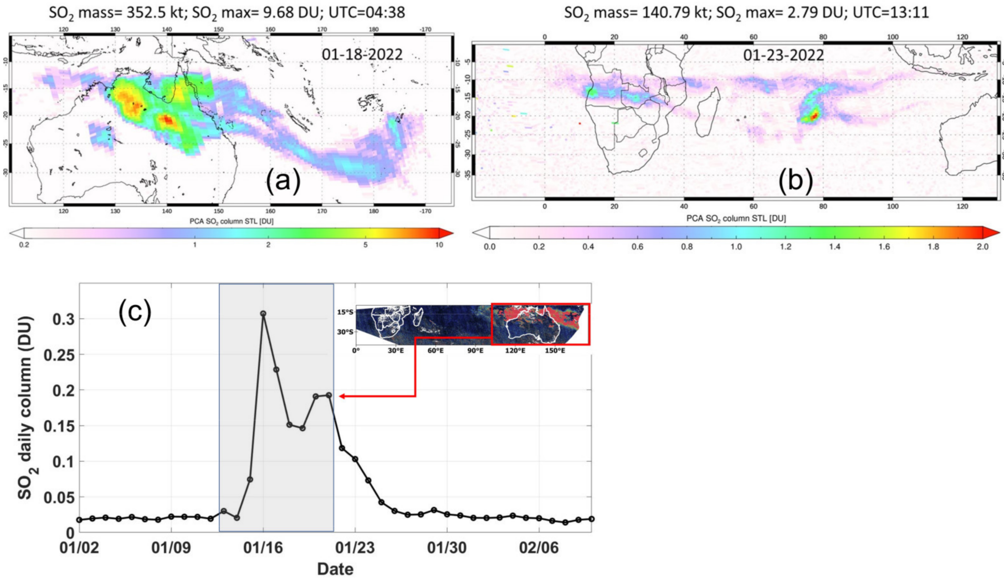


**Figure 5.** Transport of $SO_2$ observed from OMPS on (**a**) 18 January 2022 and (**b**) 23 January 2022. (**c**) OMI $SO_2$ column density time series from 1 January to 10 February 2022 over 0–40° S and 10–180° E region.

*4.4. Trend Analysis of AOD and Angstrom Parameter*

Aerosol optical depth (AOD) is an indicator of the aerosol loading in the vertical column of the atmosphere and constitutes the main parameter to assess the aerosol radiative forcing and its effects on climate. The Angstrom parameter (AP) gives information on the predominant size of suspended particles, and it is also an indicator of the relative fine mode strength. Figure 6 represents the daily MODIS AOD and aerosol Angstrom parameter over a period from 1 January to 28 February 2022. In general, the results show that higher AOD values were associated with relatively lower AP values. The higher AOD peak of 0.166 on 18 January 2022 was associated with a thick volcanic aerosol plume over Australia (see Figure 2). This was accompanied by a low AP value of 1.061, which implied the presence of coarse mode aerosols. On the other hand, higher values of AP between 1.2 and 1.4 could imply the presence of mixed aerosols [37].

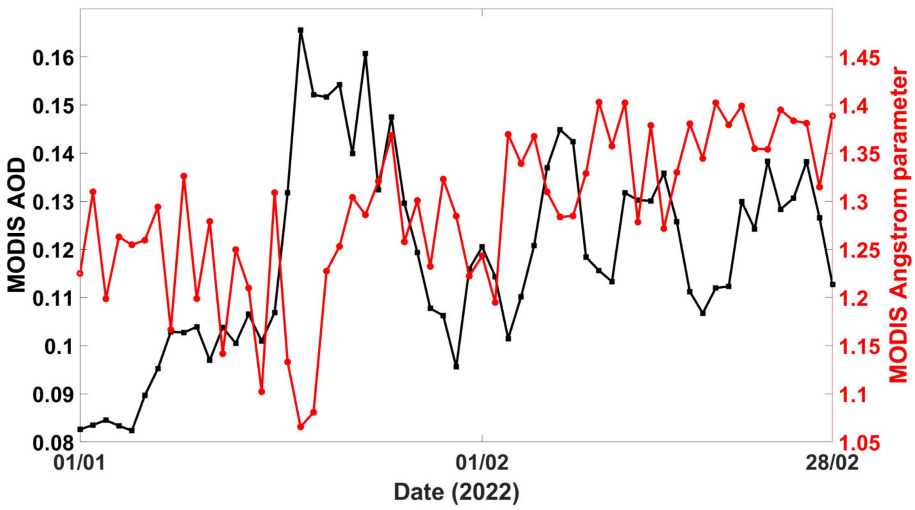


**Figure 6.** Daily evolution of MODIS AOD and aerosol Angstrom parameter during the period 1 January to 28 February 2022 from the Tonga volcanic eruption site to the southern Atlantic Ocean.

*4.5. CALIPSO Volcanic Aerosol Observations*

The CALIPSO vertical feature mask (VFM) classifies aerosols and clouds based on their physical feature [38]. Figure 7 shows the VFM with a daily consistent stratospheric feature at altitudes between 18 and 28 km classified as volcanic sulfate aerosol originating from the Tonga volcanic eruption. The eruption released matter into the stratosphere, thus increasing the volcanic sulfate aerosol loading. Furthermore, Figure 7 shows the transport of the volcanic sulphate aerosol over Australia on 19 January 2022 in a westward direction, over the Indian Ocean on 26 January 2022, and finally travelling over the RSA on 29 January and 3 February 2022. This observation agrees with the TROPOMI, which also observed the transport of $SO_2$ in the same manner. The largest volcanic sulfate aerosol plume thickness, of ~4 km, was observed on 19 January 2022 (4 days post-eruption). The thick volcanic sulphate aerosol layer in the stratosphere can affect the Earth's radiative balance by increasing the scattering of incoming solar radiation and enhancing the infrared absorption, and thus can temporarily cool the Earth's surface and troposphere [39]. Sellitto et al. [40] showed that, immediately after the eruption at the top-of-the-atmosphere and surface, volcanic aerosol cooling dominated the radiative forcing. They further showed that water vapor radiative cooling dominated the local stratospheric heating/cooling rates [40]. A moderate plume thickness of ~1 km was also observed over the RSA on 29 January 2022. This thin volcanic sulfate aerosol layer also likely had a cooling effect on the Earth's surface and the troposphere.

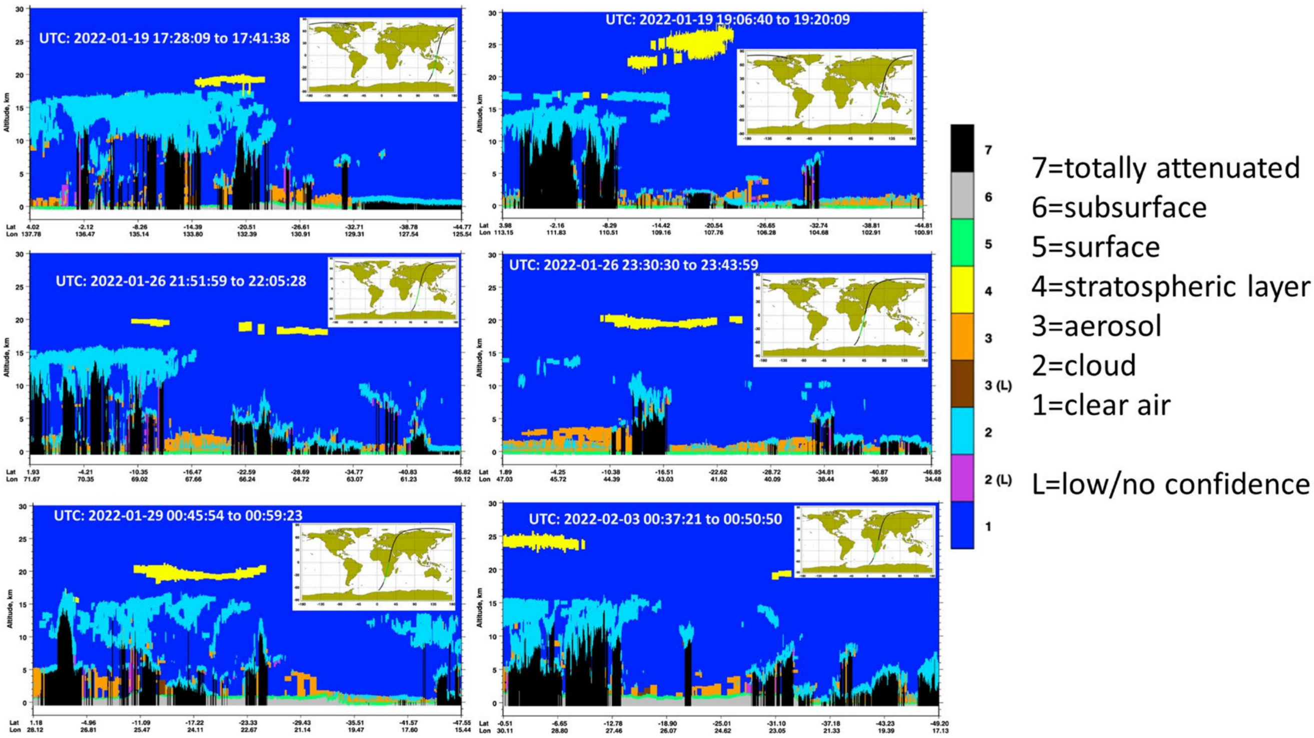


**Figure 7.** CALIPSO vertical feature mask profiles showing a consistent stratospheric layer (volcanic/sulphate aerosols) from 19 January to 3 February 2022.

## 5. Discussion and Summary

Various studies on the Tonga volcanic eruption have been conducted. For example, Kloss et al. [21] used the balloon-borne characterization method over La Réunion Island (21.1° S, 55.3° E) to observe the stratospheric aerosol plume one week after the volcanic eruption. Their observations showed sampled plumes between 19 and 25 km consisting of very small particles with radii between 0.5 and 1 µm. Li et al. [41] investigated the total electron content (TEC) variation over China due to the volcanic eruption. They observed the TEC perturbations passing over China four times after the Tonga volcano eruption. The travelling speed of the four signals were 340, 310, 301, and 264 $m\,s^{-1}$.

To our knowledge, no studies on the transport of $SO_2$ and volcanic aerosols have been conducted over South Africa. Therefore, this study intends to address that gap. The results clearly show that $SO_2$ and volcanic aerosols plume did indeed travel over the

Indian Ocean to reach South Africa by the general circulation. The TROPOMI as well as ground-based instruments (SAAQIS) in South Africa showed abnormally higher amounts of $SO_2$ in the northeastern and central parts of South Africa emanating from the volcanic eruption. Volcanic aerosols as high as 22 km in altitude were observed. Xu et al. [20] reported that large amounts of water vapor were injected into the stratosphere and were likely transported with the volcanic aerosols. The increase in water vapor in the upper troposphere and lower stratosphere (UTLS) would lead to radiative cooling and induce warming at the surface. Charlesworth et al. [42] also showed that the abundance of water vapor in the UTLS levels are sensitivity of the atmospheric circulation.

From the TROPOMI measurements, the $SO_2$ column density (mol/m$^2$) values were at 0.0040 (Tonga), 0.0012 (Australia), 0.0055 (Indian Ocean), and 0.0007 (South Africa). The observed $SO_2$ values over South Africa were around 5.7 times weaker than those observed over Tonga and 1.7 times weaker than those observed over the Indian Ocean. The decrease in the $SO_2$ column density was due to the oxidation of $SO_2$ to gaseous sulfuric acid which further condensed into $H_2SO_4$–$H_2O$ liquid aerosol, which is expected [43].

The conversion of $SO_2$ to $H_2SO_4$, which condenses rapidly in the stratosphere to form fine sulfate aerosols, is the most significant climate impact from volcanic injections into the stratosphere. This process increases the reflection of radiation from the sun back into space, which reduces the impact of global warming by cooling the Earth's lower atmosphere [44]. Thus, monitoring the distribution of $SO_2$ and sulfate aerosols after a volcanic eruption is vital. High spatial and temporal resolution observations are key to enabling the observation of $SO_2$ and sulphate aerosols and providing better concentration estimates that can be used as inputs into climatic models. TROPOMI datasets are good at determining the transport and total column density of $SO_2$. In conjunction with CALIPSO data, they provide a more accurate scenario of the direction and height of the volcanic constituents' travel. The transport of the volcanic constituents analyzed for this study was limited to the RSA; however, the time scale could be extended to observe how far the $SO_2$ and sulfate aerosols travelled.

**Author Contributions:** Conceptualization, L.S. and V.S.; methodology, L.S.; software, L.S.; validation, L.S., V.S. and K.X; formal analysis, L.S.; writing—original draft preparation, L.S.; writing—review and editing, V.S. and K.X. All authors have read and agreed to the published version of the manuscript.

**Funding:** The APC was funded by the South African National Space Agency.

**Institutional Review Board Statement:** Not applicable.

**Informed Consent Statement:** Not applicable.

**Data Availability Statement:** The datasets generated and/or analyzed during the current study are available from the corresponding author on reasonable request.

**Acknowledgments:** We thank the Atmospheric Science Data Center at NASA Langley Research Center for archiving and hosting CALIPSO data. We further thank and acknowledge the ESA for the Sentinel-5P/TROPOMI data. The authors acknowledge the GES-DISC Interactive Online Visualization and Analysis Infrastructure (Giovanni) for providing the OMI data. We acknowledge the use of OMPS data.

**Conflicts of Interest:** The authors declare no conflict of interest.

## References

1. WHO. Volcanic Eruptions. 2022. Available online: https://www.who.int/health-topics/volcanic-eruptions#tab=tab_3 (accessed on 21 February 2022).
2. Vernier, J.P.; Fairlie, T.D.; Deshler, T.; Natarajan, M.; Knepp, T.; Foster, K.; Wienhold, F.G.; Bedka, K.M.; Thomason, L.; Trepte, C. In situ and space-based observations of the Kelud volcanic plume: The persistence of ash in the lower stratosphere. *J. Geophys. Res. Atmos.* **2016**, *121*, 11104–11118. [CrossRef]
3. Stone, K.A.; Solomon, S.; Kinnison, D.E.; Pitts, M.C.; Poole, L.R.; Mills, M.J.; Schmidt, A.; Neely, R.R., III; Ivy, D.; Schwartz, M.J.; et al. Observing the impact of Calbuco volcanic aerosols on South Polar ozone depletion in 2015. *J. Geophys. Res. Atmos.* **2017**, *122*, 11862–11879. [CrossRef]

4. Lopes, F.; Silva, J.; Marrero, J.; Taha, G.; Landulfo, E. Synergetic Aerosol Layer Observation After the 2015 Calbuco Volcanic Eruption Event. *Remote Sens.* **2019**, *11*, 195. [CrossRef]
5. Sangeetha, S.K.; Sivakumar, V.; Gebreslasie, M. Long-range transport of $SO_2$ over South Africa: A case study of the Calbuco volcanic eruption in April 2015. *Atmos. Environ.* **2018**, *185*, 78–90. [CrossRef]
6. Shikwambana, L.; Sivakumar, V. Long-range transport of volcanic aerosols over South Africa: A case study of the Calbuco volcanic eruption in Chile during April 2015. *S. Afr. Geogr. J.* **2018**, *100*, 349–363. [CrossRef]
7. Bègue, N.; Shikwambana, L.; Bencherif, H.; Pallotta, J.; Sivakumar, V.; Wolfram, E.; Mbatha, N.; Orte, F.; Du Preez, D.J.; Ranaivombola, M.; et al. Statistical analysis of the long-range transport of the 2015 Calbuco volcanic plume from ground-based and space-borne observations. *Ann. Geophys.* **2020**, *38*, 395–420. [CrossRef]
8. Kloss, C.; Berthet, G.; Sellitto, P.; Ploeger, F.; Taha, G.; Tidiga, M.; Eremenko, M.; Bossolasco, A.; Jégou, F.; Renard, J.-B.; et al. Stratospheric aerosol layer perturbation caused by the 2019 Raikoke and Ulawun eruptions and their radiative forcing. *Atmos. Chem. Phys.* **2021**, *21*, 535–560. [CrossRef]
9. Shin, D.; Müller, D.; Lee, K.; Shin, S.; Kim, Y.J.; Song, C.K.; Noh, Y.M. Lidar observations of Nabro volcano aerosol layers in the stratosphere over Gwangju, Korea. *Atmos. Chem. Phys. Discuss.* **2015**, *15*, 1171–1191. [CrossRef]
10. Krotkov, N.A.; McLinden, C.A.; Li, C.; Lamsal, L.N.; Celarier, E.A.; Marchenko, S.V.; Swartz, W.H.; Bucsela, E.J.; Joiner, J.; Duncan, B.N.; et al. Aura OMI observations of regional $SO_2$ and $NO_2$ pollution changes from 2005 to 2015. *Atmos. Chem. Phys.* **2016**, *16*, 4605–4629. [CrossRef]
11. Theys, N.; Hedelt, P.; De Smedt, I.; Lerot, C.; Yu, H.; Vlietinck, J.; Pedergnana, M.; Arellano, S.; Galle, B.; Fernandez, D.; et al. Global monitoring of volcanic $SO_2$ degassing with unprecedented resolution from TROPOMI onboard Sentinel-5 Precursor. *Sci. Rep.* **2019**, *9*, 2643. [CrossRef]
12. Koukouli, M.-E.; Michailidis, K.; Hedelt, P.; Taylor, I.A.; Inness, A.; Clarisse, L.; Balis, D.; Efremenko, D.; Loyola, D.; Grainger, R.G.; et al. Volcanic $SO_2$ Layer Height by TROPOMI/S5P; validation against IASI/MetOp and CALIOP/CALIPSO observations. *Atmos. Chem. Phys.* **2022**, *22*, 5665–5683. [CrossRef]
13. Carn, S.; Fioletov, V.; McLinden, C.A.; Li, C.; Krotkov, N.A. A decade of global volcanic $SO_2$ emissions measured from space. *Sci. Rep.* **2017**, *7*, 44095. [CrossRef]
14. Zerefos, C.S.; Eleftheratos, K.; Kapsomenakis, J.; Solomos, S.; Inness, A.; Balis, D.; Redondas, A.; Eskes, H.; Allaart, M.; Amiridis, V.; et al. Detecting volcanic sulfur dioxide plumes in the Northern Hemisphere using the Brewer spectrophotometers, other networks, and satellite observations. *Atmos. Chem. Phys.* **2017**, *17*, 551–574. [CrossRef]
15. Bourassa, A.E.; Zawada, D.J.; Rieger, L.A.; Warnock, T.W.; Toohey, M.; Degenstein, D.A. Tomographic retrievals of Hunga Tonga-Hunga Ha'apai volcanic aerosol. *Geophys. Res. Lett.* **2023**, *50*, e2022GL101978. [CrossRef]
16. Ge, C.; Wang, J.; Carn, S.; Yang, K.; Ginoux, P.; Krotkov, N. Satellite-based global volcanic $SO_2$ emissions and sulfate direct radiative forcing during 2005–2012. *J. Geophys. Res. Atmos.* **2016**, *121*, 3446–3464. [CrossRef]
17. Wright, R.; Flynn, L.; Garbeil, H.; Harris, A.; Pilger, E. Automated volcanic eruption detection using MODIS. *Remote Sens. Environ.* **2002**, *82*, 135–155. [CrossRef]
18. Zhang, Y.; Tsou, J.Y.; Huang, Z.; Hu, J.; Yim, W. Monitoring of the 2008 Chaitén eruption cloud using MODIS data and its impacts. In *Geospatial Technology—Environmental and Social Applications*; Imperatore, P., Pepe, A., Eds.; IntechOpen: London, UK, 2016. [CrossRef]
19. Global Volcanism Program. Report on Hunga Tonga-Hunga Ha'apai (Tonga). In *Bulletin of the Global Volcanism Network*; Smithsonian Institution: Washington, DC, USA, 2022; Volume 40, p. 1.
20. Xu, J.; Li, D.; Bai, Z.; Tao, M.; Bian, J. Large Amounts of Water Vapor Were Injected into the Stratosphere by the Hunga Tonga–Hunga Ha'apai Volcano Eruption. *Atmosphere* **2022**, *13*, 912. [CrossRef]
21. Tilstra, L.G.; de Graaf, M.; Wang, P.; Stammes, P. In-orbit Earth reflectance validation of TROPOMI on board the Sentinel-5 Precursor satellite. *Atmos. Meas. Tech.* **2020**, *13*, 4479–4497. [CrossRef]
22. Verhoelst, T.; Compernolle, S.; Pinardi, G.; Lambert, J.-C.; Eskes, H.J.; Eichmann, K.-U.; Fjæraa, A.M.; Granville, J.; Niemeijer, S.; Cede, A.; et al. Ground-based validation of the Copernicus Sentinel-5P TROPOMI NO2 measurements with the NDACC ZSL-DOAS, MAX-DOAS and Pandonia global networks. *Atmos. Meas. Tech.* **2021**, *14*, 481–510. [CrossRef]
23. Boersma, K.F.; Bucsela, E.; Brinksma, E.J.; Gleason, J.F. NO2. In *OMI Algorithm Theoretical Basis Document, OMI Trace Gas Algorithms, ATBOMI-04, Version 2.0*; Chance, K., Ed.; NASA: Washington, DC, USA, 2002; Volume 4, pp. 13–36. Available online: https://ozoneaq.gsfc.nasa.gov/media/docs/ATBD-OMI-04.pdf (accessed on 2 August 2023).
24. Bucsela, E.J.; Celarier, E.A.; Wenig, M.O.; Gleason, J.F.; Veefkind, J.P.; Boersma, K.F.; Brinksma, E.J. Algorithm for NO2 vertical column retrieval from the ozone monitoring instrument. *IEEE Trans. Geosci. Remote Sens.* **2006**, *44*, 1245–1258. [CrossRef]
25. Levelt, P.F.; Hilsenrath, E.; Leppelmeier, G.W.; van den Oord, G.H.J.; Bhartia, K.; Tamminen, J.; de Haan, J.F.; Veefkind, J.P. Science objectives of the ozone monitoring instrument. *IEEE Trans. Geosci. Remote Sens.* **2006**, *44*, 1199–1208. [CrossRef]
26. Levelt, P.F.; Joiner, J.; Tamminen, J.; Veefkind, J.P.; Bhartia, P.K.; Stein Zweers, D.C.; Duncan, B.N.; Streets, D.G.; Eskes, H.; van der Ronald, A.; et al. The Ozone Monitoring Instrument: Overview of 14 years in space. *Atmos. Chem. Phys.* **2018**, *18*, 5699–5745. [CrossRef]
27. Flynn, L.E.; Seftor, C.J.; Larsen, J.C.; Xu, P. The ozone mapping and profiler suite. In *Earth Science Satellite Remote Sensing*; Qu, J.J., Gao, W., Kafatos, M., Murphy, R.E., Salomonson, V.V., Eds.; Springer: Berlin/Heidelberg, Germany, 2006. [CrossRef]

28. Yang, K.; Dickerson, R.R.; Carn, S.A.; Ge, C.; Wang, J. First observations of $SO_2$ from the satellite Suomi NPP OMPS: Widespread air pollution events over China. *Geophys. Res. Lett.* **2013**, *40*, 4957–4962. [CrossRef]
29. Winker, D.M.; Vaughan, M.A.; Omar, A.; Hu, Y.; Powell, K.A.; Liu, Z.; Hunt, W.H.; Young, S.A. Overview of the CALIPSO mission and CALIOP data processing algorithms. *J. Atmos. Ocean. Technol.* **2009**, *26*, 2310–2323. [CrossRef]
30. Winker, D.M.; Pelon, J.R.; McCormick, M.P. The CALIPSO mission: Spaceborne lidar for observation of aerosols and clouds. In Proceedings of the 3rd International Asia-Pacific Environmental Remote Sensing—Remote Sensing of the Atmosphere, Ocean, Environment, and Space, Hangzhou, China, 23–27 October 2002; pp. 1–11. [CrossRef]
31. Winker, D.; Pelon, J.; Coakley, J., Jr.; Ackerman, S.; Charlson, R.; Colarco, P.; Flamant, P.; Fu, Q.; Hoff, R.; Kittaka, C. The CALIPSO mission: A global 3d view of aerosols and clouds. *Bull. Am. Meteorol. Soc.* **2010**, *91*, 1211–1230. [CrossRef]
32. Gwaze, P.; Mashele, S.H. South African Air Quality Information System (SAAQIS) mobile application tool: Bringing real time state of air quality to South Africans. *Clean Air J.* **2018**, *28*, 3. [CrossRef]
33. Pretorius, I.P.; Piketh, S.; Burger, R.; Neomagus, H. A perspective on South African coal fired power station emissions. *J. Energy S. Afr.* **2015**, *26*, 27–40. [CrossRef]
34. Shikwambana, L.; Kganyago, M.; Mhangara, P. Temporal Analysis of Changes in Anthropogenic Emissions and Urban Heat Islands during COVID-19 Restrictions in Gauteng Province, South Africa. *Aerosol Air Qual. Res.* **2021**, *21*, 200437. [CrossRef]
35. Gorkavyi, N.; Krotkov, N.; Li, C.; Lait, L.; Colarco, P.; Carn, S.; DeLand, M.; Newman, P.; Schoeberl, M.; Taha, G.; et al. Tracking aerosols and $SO_2$ clouds from the Raikoke eruption: 3D view from satellite observations. *Atmos. Meas. Tech.* **2021**, *14*, 7545–7563. [CrossRef]
36. Von Savigny, C.; Timmreck, C.; Buehler, S.A.; Burrows, J.P.; Giorgetta, M.; Hegerl, G.; Horvath, A.; Hoshyaripour, G.A.; Hoose, C.; Quaas, J.; et al. The Research Unit Vol Impact: Revisiting the volcanic impact on atmosphere and climate—Preparations for the next big volcanic eruption. *Meteorol. Z.* **2020**, *29*, 3–18. [CrossRef]
37. Shikwambana, L.; Kganyago, M. Trends in atmospheric pollutants from oil refinery processes: A case study over the United Arab Emirates. *Remote Sens. Lett.* **2020**, *11*, 590–597. [CrossRef]
38. Vaughan, M.; Young, S.; Winker, D.M.; Powell, K.; Omar, A.; Liu, Z.; Hu, Y.; Hostetler, C. Fully automated analysis of space-based lidar data: An overview of the CALIPSO retrieval algorithms and data products. *Laser Radar Tech. Atmos. Sens.* **2004**, *5575*, 16–30. [CrossRef]
39. Naik, V.; Horowitz, L.W.; Schwarzkopf, D.M.; Lin, M. Impact of volcanic aerosols on stratospheric ozone recovery. *J. Geophys. Res. Atmos.* **2017**, *122*, 9515–9528. [CrossRef]
40. Sellitto, P.; Podglajen, A.; Belhadji, R.; Boichu, M.; Carboni, E.; Cuesta, J.; Duchamp, C.; Kloss, C.; Siddans, R.; Bègue, N.; et al. The unexpected radiative impact of the Hunga Tonga eruption of 15th January 2022. *Commun. Earth Environ.* **2022**, *3*, 288. [CrossRef]
41. Li, T.; Gao, Y.; Chen, C.-H.; Zhang, X.; Sun, Y.-Y. Ionospheric disturbances observed over China after 2022 January 15 Tonga volcano eruption. *Geophys. J. Int.* **2023**, *235*, 909–919. [CrossRef]
42. Charlesworth, E.; Plöger, F.; Birner, T.; Baikhadzhaev, R.; Abalos, M.; Abraham, N.L.; Akiyoshi, H.; Bekki, S.; Dennison, F.; Jöckel, P.; et al. Stratospheric water vapor affecting atmospheric circulation. *Nat. Commun.* **2023**, *14*, 3925. [CrossRef] [PubMed]
43. Bègue, N.; Vignelles, D.; Berthet, G.; Portafaix, T.; Payen, G.; Jégou, F.; Benchérif, H.; Jumelet, J.; Vernier, J.-P.; Lurton, T.; et al. Long-range transport of stratospheric aerosols in the Southern Hemisphere following the 2015 Calbuco eruption. *Atmos. Chem. Phys.* **2017**, *17*, 15019–15036. [CrossRef]
44. Laakso, A.; Korhonen, H.; Romakkaniemi, S.; Kokkola, H. Radiative and climate effects of stratospheric sulfur geoengineering using seasonally varying injection areas. *Atmos. Chem. Phys.* **2017**, *17*, 6957–6974. [CrossRef]